A Wide-Beam Base Station Antenna with Modular Radiator for Reconfigurability

Joshua W. Shehan[1, 2, *] and Ryan S. Adams[2]

Abstract—This paper presents a reconfigurable wide-beam antenna with a modular main radiator for base station applications. The addition of new spectrum and the path to 5G create unique antenna requirements in terms of patterns and impedance matching capabilities. The antenna in this paper exhibits a wide azimuth beamwidth up to approximately 180° and implements a modular approach where the antenna can be reconfigured for impedance matching requirements. Two configurations of the wide-beam antenna are presented; the first configuration covers the 1.7–2.7 GHz band for 3G/4G/LTE applications where multiple wireless carriers would use the same antenna as a neutral site. This antenna provides wide-beam operation and a 10-dB return loss from approximately 1.64–2.76 GHz. The measured return loss over the 1.7–2.7 GHz band is better than 13 dB. A second configuration of the antenna is tuned for performance from 1.9–2.4 GHz where measured return loss better than 19 dB is achieved in this band. Simulated and measured return losses and patterns are presented that show very good agreement between simulation and measurement, and thorough parametric pattern analysis is presented for the baseline antenna configuration.

1. INTRODUCTION

One of the greatest challenges facing today's wireless carriers is providing the desired network coverage and capacity in urban environments where the traditional macro cell approach does not work. The predominant trend to address this challenge is the deployment of distributed antenna system (DAS) and small cell antennas where a large number of relatively low-gain antennas are deployed throughout the operating environment [1]. However, it can be difficult to find mounting locations where the antennas integrate unobtrusively into the surrounding architecture. The aesthetics of the antenna are important, and zoning restrictions often limit antenna mounting options. Depending on the antenna location and desired coverage area, small cell antennas may also have unique pattern requirements. For example, an antenna mounted to the side of a building requires wide-beam radiation patterns up to 180° for users outside of the building, but the antenna should not radiate into the building. Radiation into the building may create interference between the outdoor base station antenna and an indoor wireless system.

Wide-beam antennas are of interest for various applications. Numerous wide-beam antennas with circular polarization have been presented primarily for satellite communication systems [2–7]. Additionally, several wide-beam elements have been proposed for phased array applications where wide beamwidth at the element level enables wide scan capability on the array [8–13]. Other antennas have been presented for wide-beam coverage that are not necessarily tailored to a specific application. The authors in [14] present a wide-beam antenna consisting of a monopole attached to a wedge-shaped reflector. A wide-beam dielectric resonator antenna with a high dielectric material is proposed in [15].

A wide-beam antenna for large platforms is presented in [16] where the antenna is mounted to the roof of a vehicle. The authors of [17] present a dual polarized base station antenna array exhibiting wide beamwidth from roughly 1.9–2.2 GHz. A variation of a monopole antenna is presented in [18] that exhibits broadband, wide-beam performance. Pattern reconfigurable wide-beam antenna elements are presented in [19, 20]. The element in [12] is also pattern reconfigurable, but the antenna does not maintain wide beam performance for the different operating modes. Note the wide-beam antennas found in the literature are not shown to be easily reconfigured for changes in the operating frequency while maintaining consistent wide-beam performance.

This paper presents a reconfigurable, wide-beam antenna (patent pending) designed to cover a maximum broadband frequency range of approximately 1.7–2.7 GHz for 3G/4G/LTE with a co-polarized (co-pol) azimuth half-power beamwidth (az-HPBW) between $\sim 142°$–$180°$. The antenna is comprised of a sleeve monopole, a grounded reflector, and a parasitic director where the main radiator of the sleeve monopole is designed in a modular fashion. This allows the antenna to be reconfigured depending on the spectrum requirements of the antenna. The broadband antenna can be used for multiple wireless carriers serving as a neutral host, but a second main radiator is presented that is optimized for operation over a more limited bandwidth of approximately 1.9–2.4 GHz. This design is useful where a single wireless carrier may be operating over a limited bandwidth. The design approach along with simulated and measured data for the two configurations of the wide-beam antenna are presented. Parametric analyses for the radiation patterns are also presented.

2. WIDE-BEAM ANTENNA WITH MODULAR MAIN RADIATOR

2.1. Broadband Antenna — Configuration A

The wide-beam antenna presented in this paper is composed of a sleeve monopole, a parasitic director, and a grounded reflector as shown in Fig. 1. Two configurations of the antenna are presented in this paper. The broadband configuration (configuration A) is presented first.

The foundation of the antenna is the sleeve monopole which has received attention in recent years
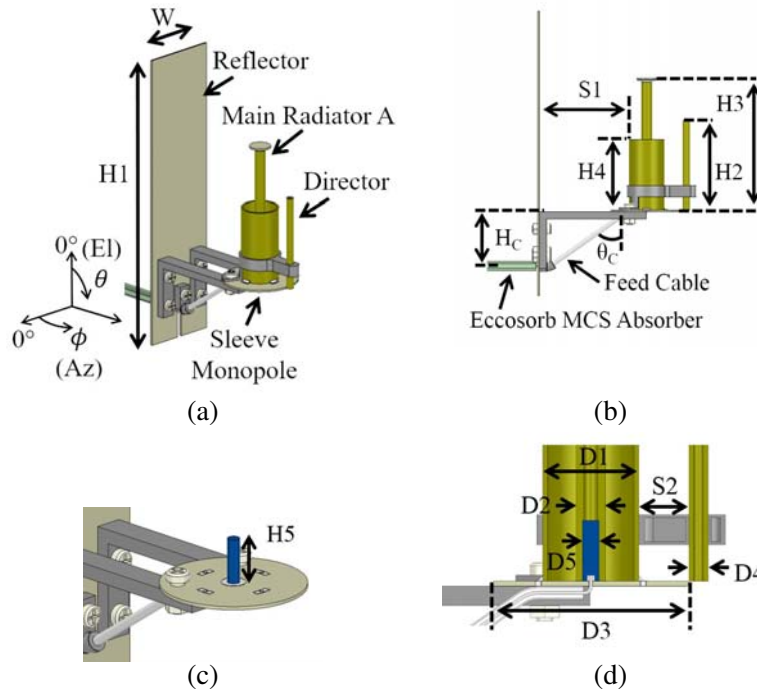
Figure 1. Antenna configuration A isometric view (a), side view (b), threaded rod placement (c), and split view (d).

as a wideband, omnidirectional antenna [21–23]. The sleeve monopole is generally composed of an outer sleeve, a main radiator, and a ground plane which is realized as a printed circuit board (PCB) in this case. A loading disk PCB with a copper diameter of 8.5 mm is soldered to the top of the brass main radiator for impedance matching at the lower end of the operating band. The loading disk and the ground PCB are made of 0.762 mm Isola 680 ($\epsilon_r = 3.38$, $\tan \delta = 0.0035$), and the copper cladding includes an immersion tin finish that is assumed to give a total metal thickness of ~ 0.06 mm. The ground PCB has a copper ground diameter given by variable $D3$ and also includes four plated through holes acting as vias to connect solder pads on the top layer to ground on the bottom layer. The brass sleeve is soldered to these pads to provide a ground connection for the sleeve. The antenna is fed through an RG-405 coaxial cable where the outer conductor of the cable is soldered to the bottom side of the ground PCB, and the center pin is fed through a non-plated through hole and soldered to a 5.45-mm diameter feed pad on the top side of the ground PCB. A 10-mm long brass m3 threaded rod is also soldered to the feed pad. This threaded rod enables modularity so that the main radiator may be changed to provide antenna tuning as is demonstrated later in this paper. The portion of the feed cable extending past the reflector is wrapped with four flat sheets of 1-mm thick Eccosorb MCS RF absorber modeled with $\epsilon_r = 38$, $\tan \delta_e = 0.01$, $\mu_r = 4$, and $\tan \delta_m = 0.75$ [24].

The reflector is used to give the sleeve monopole directionality where the size and position of the reflector can be used to control the azimuth beamwidth. Like the ground PCB and loading disk, the reflector is made of Isola 680 PCB material where the copper is completely etched away from one side, and the copper side is grounded through the RG-405 coaxial feed cable. The angle, θ_c, and height, H_C, are used primarily for elevation pattern control. The width and height of the reflector copper are given by variables W and $H1$, respectively. Note that the dielectric extends 0.254 mm past the edges of the copper for the reflector PCB, ground PCB, and loading disk PCB. This maintains clean edges on the copper when the boards are cut out during fabrication.

The support structures to hold parts in place are 3D printed ABS from a Fusion 3 FDM 3D printer. The material is characterized using an in-house coaxial shorted transmission line test fixture, and the dielectric material properties are extracted. The extracted ϵ_r is between roughly 2.48–2.5, and the extracted $\tan \delta$ is between roughly 0.004 and 0.008. For simulation purposes, this paper assumes the support material to have $\epsilon_r = 2.5$ and a loss tangent of $\tan \delta = 0.007$. L-shaped mounting brackets and the director support are 3D printed with wall thicknesses between ~ 0.5–0.8 mm and a 5% infill so that these structures are essentially hollow. This minimizes the impact of the dielectric properties on the antenna performance. Note the portion of the director support in contact with the sleeve is designed as a solid piece with a thickness of 1 mm. The support structures are secured to the antenna with plastic fasteners.

2.1.1. Benefit of the Parasitic Director

To illustrate the benefit of the director, antenna A is compared to a wide-beam antenna without a director in Fig. 2. Note that the wide-beam antenna without the director is designed to provide a peak co-pol az-HPBW of $\sim 180°$ with an acceptable impedance match where return loss is better than 10 dB from 1.68–2.76 GHz. In some cases, base station antennas are mechanically tilted to avoid interference with neighboring sites or improve service for users in a particular coverage area. Therefore, it is desirable to minimize antenna pattern variation over frequency. Without the director, the $\phi = 90°$ -10-dB crossover (the point where the co-pol elevation pattern is reduced to 10 dB below its peak value) varies from an elevation angle of $\theta \simeq 33°$ at 1.7 GHz to an elevation angle of $\theta \simeq 58°$ at 2.7 GHz. This amount of variation may be unacceptable for situations where the antenna is mechanically tilted. The director is found to improve the -10-dB crossover variation from an elevation angle of $\theta \simeq 35°$ at 1.7 GHz to an elevation angle of $\theta \simeq 44°$ at 2.7 GHz.

The director is also found to reduce the variation in azimuth beamwidth over the 1.7–2.7 GHz band. The simulated az-HPBW for the antenna without the director varies from $\sim 124°$–180°, and the az-HPBW for the antenna with the director varies from $\sim 142°$–180°. Note that the presence of the director requires some dimensional variation in the antenna design, but this also provides an additional tuning feature for the antenna.
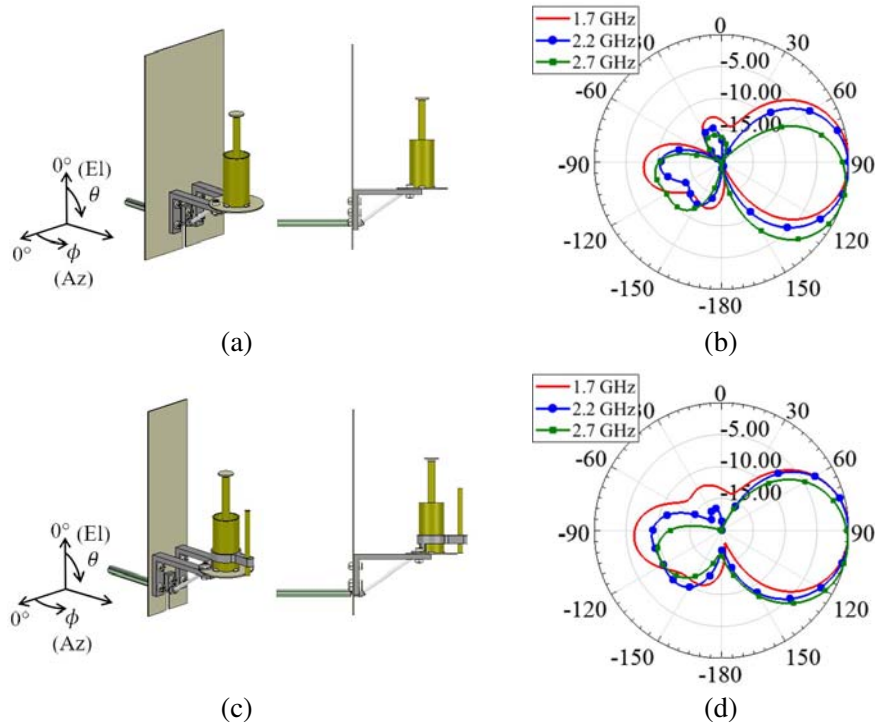
Figure 2. Comparison of the wide-beam antenna with no director (a) and its co-pol elevation patterns at $\phi = 90°$ (b) to the wide-beam antenna with a parasitic director (c) and its co-pol elevation patterns at $\phi = 90°$ (d).

2.1.2. Input Match Parametric Study

The sleeve height and main radiator height are used to fine tune the antenna match at the upper and lower ends of the operating band. A parametric study on the impacts of the sleeve height and main radiator height are presented in Fig. 3 where it is apparent that the main radiator height can be used primarily for adjustment at the lower part of the operating band, and the sleeve height can be used primarily for adjustment at the upper part of the operating band. Notice that both parameters also impact the match over the central part of the operating band. For this analysis, the antenna is set to the nominal design variables listed in Table 1 aside from the variable under investigation.
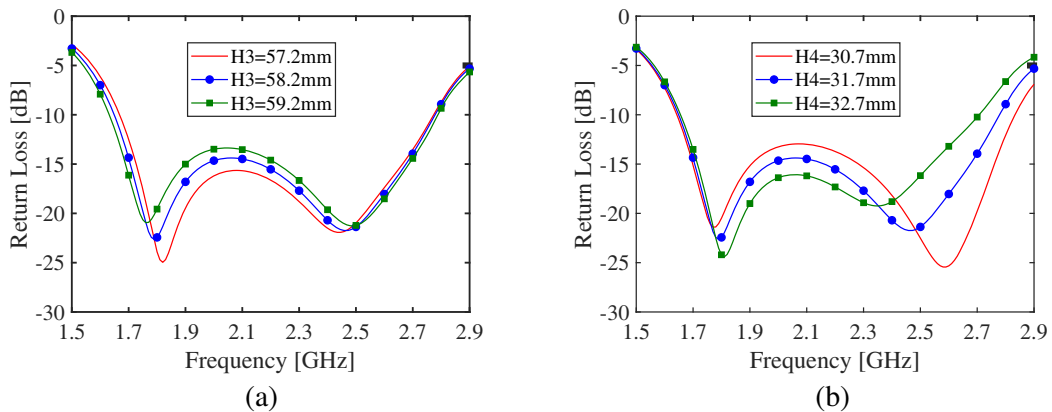
Figure 3. Effects of main radiator height, $H3$, (a) and sleeve height, $H4$, (b) on the impedance match for antenna configuration A.

Table 1. Nominal design values for antenna configuration A.

Variable	mm	Variable	mm	Variable	mm/deg
W	31.75	$H5$	10	$D3$	31.75
$H1$	127	$S1$	40.1	$D4$	3.175
$H2$	40	$S2$	8.3	$D5$	2.75
$H3$	58.2	$D1$	15.875	θ_C [deg]	55
$H4$	31.7	$D2$	4.7625	H_C	23.2

2.2. Narrow Band Antenna with Modified Main Radiator — Configuration B

The previous section presents a modular main radiator where a threaded rod is used as a means to change the main radiator and reconfigure the antenna performance. This feature can be used to tune the antenna for specific frequency bands. For instance, the antenna could be used as a neutral host where different wireless carriers that have different operating bands use the same antenna. In this case, the antenna may need to cover the full spectrum from 1.7–2.7 GHz. However, in some cases, the antenna might only serve a single carrier requiring limited bandwidth. In this case, it is desirable that the antenna is optimized for the required bandwidth with disregard for other bands that are not used.

Here, a main radiator is designed to provide excellent return loss (better than $\sim$ 22 dB) from 1.9–2.4 GHz while sacrificing performance from 1.7–1.9 GHz and 2.4–2.7 GHz. This way, reflections are minimized in the desired operating band and the overall antenna system can be optimized for a single wireless carrier. This configuration is referred to as antenna configuration B. The main radiator is shortened, and a capacitive disk is added to the main radiator as shown in Fig. 4 with dimensions listed in Table 2. This disk is punched from a sheet of 0.127-mm brass foil and soldered to the main radiator, but the entire structure could be machined from a solid piece of brass. Other than the dimensions listed in Table 2, the antenna dimensions match those listed in Table 1 for antenna A. Note that the antenna
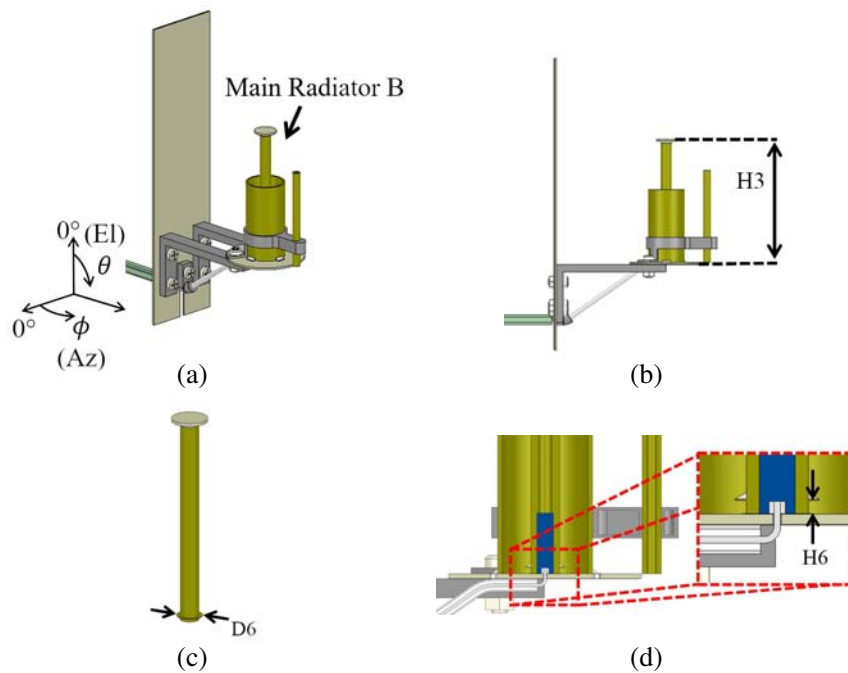
Figure 4. Antenna configuration B isometric view (a), side view (b), main radiator (c), and split view (d).

Table 2. Nominal design values for antenna configuration B.

Variable	mm	Variable	mm	Variable	mm
$H3$	52.9	$D6$	6.4975	$H6$	1

can be tuned to cover various portions of the operating band with modification of the main radiator and/or dielectric loading in the sleeve.

2.2.1. Input Match Parametric Study

With the sleeve height fixed and the main radiator height reduced to 52.9 mm, the effects of the capacitive disk on the input match are investigated here. The nominal design values are listed in Table 2. Fig. 5 indicates that the size and offset of the capacitive disk can be used to adjust the upper end of the operating band. Without the capacitive disk, the return loss exhibits a null near 1.9 GHz, but the return loss is degraded near 2.4 GHz. This is implied by Fig. 5 where reducing the diameter $D6$ or increasing the height $H6$ degrades the match near 2.4 GHz. Alternatively, increasing the diameter $D6$ or reducing the height $H6$ increases the capacitance near the base of the main radiator. This provides a better match near 2.4 GHz and provides slightly more bandwidth, but it also degrades the match in the center of the band.

(a)   (b)
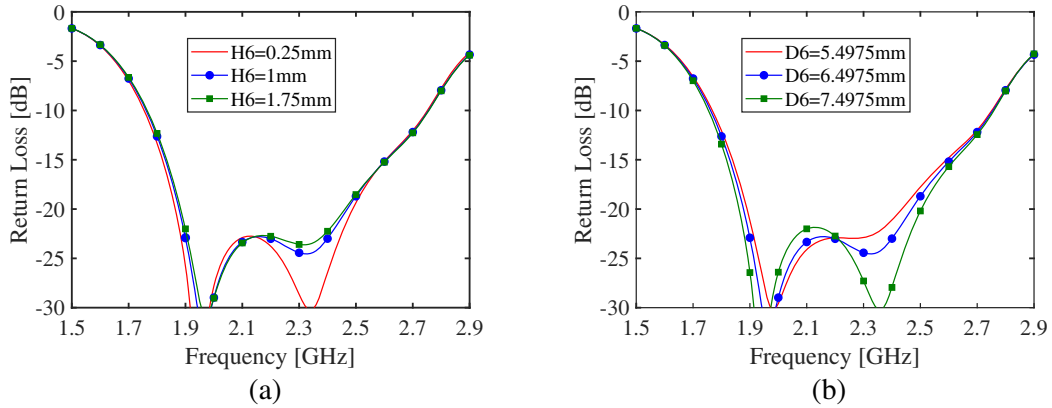
Figure 5. Effects of capacitive disk height, $H6$, (a) and radius, $D6$, (b) on impedance match for antenna configuration B.

3. PATTERN PARAMETRIC STUDY

A parametric study of the radiation patterns is presented here. The effects studied in this analysis apply to both configurations presented above, but the analysis is conducted using configuration A since it is the most general configuration. The reflector width and separation can be used to control azimuth beamwidth, and their impacts are shown in Fig. 6. Note that the azimuth patterns shown here are plotted through the peak of the co-pol main beam.

The simulated azimuth beamwidths at 2.2 GHz are compared for reflector widths of 21.75 mm, 31.75 mm, and 41.75 mm in Fig. 6(a) where it is shown that variations of up to 20 mm in the reflector width do not have significant impacts on the azimuth patterns. The az-HPBW only varies from $\sim 184°$ with $W = 21.75$ mm to $\sim 173°$ with $W = 41.75$ mm. There is a small impact on the beam squint at 2.2 GHz where the co-pol beam peak occurs at elevation angles of $\theta \simeq 91°$, 93°, and 94° for $W = 21.75$ mm, 31.75 mm, and 41.75 mm respectively. The reflector spacing has a more significant impact on the azimuth beamwidths as indicated in Fig. 6(b) where the simulated azimuth beamwidths at 2.2 GHz are compared for reflector spacings of 35.1 mm, 40.1 mm, and 45.1 mm. The az-HPBW varies

from $\sim 162°$ with $S1 = 35.1$ mm to $\sim 194°$ with $S1 = 45.1$ mm. The reflector spacing also has a small impact on the beam squint at 2.2 GHz where the co-pol beam peak occurs at $\theta \simeq 91°$, $93°$, and $95°$ for $S1 = 35.1$ mm, 40.1 mm, and 45.1 mm respectively. Increasing the reflector height can provide a deeper null at the lower part of the operating band and improve the spread on the -10-dB crossover angle, but this comes at the expense of increased antenna height. For this paper, the reflector height, $H1$, is chosen to be 127 mm.

The impacts of the director and feed cable on the elevation pattern are investigated in Figs. 7–9. The antenna presented in this paper is designed primarily for wide azimuth beamwidth, but elevation pattern control is not trivial. Where the azimuth patterns are determined largely by the reflector configuration, the elevation pattern performance is determined by the parasitic director, feed cable, and the overall geometry of the sleeve monopole. Fig. 7 shows the impact of the director length, $H2$. By design, the director length has little impact on the patterns at 1.7 GHz, but it can have a significant impact on the elevation patterns at 2.7 GHz as shown in Fig. 7(b). A director length of 45 mm significantly reduces squint in elevation, but it also creates additional unwanted radiation above the main beam. On the other hand, a director length of 35 mm does not provide the desired improvement in elevation pattern performance where the -10-dB crossover is $\sim 51°$ in the $\phi = 90°$ plane.

The impacts of the director spacing are shown in Fig. 8. Similar to the director length, the director spacing has little impact on the patterns at 1.7 GHz, but this spacing can have a dramatic impact on the patterns at 2.7 GHz. Placing the director too close can significantly degrade the elevation pattern shape as indicated in Fig. 8(b) where a large amount of radiation is pushed upward above the main beam. However, moving the director in the other direction away from the sleeve does not have a tremendous

(a)   (b)
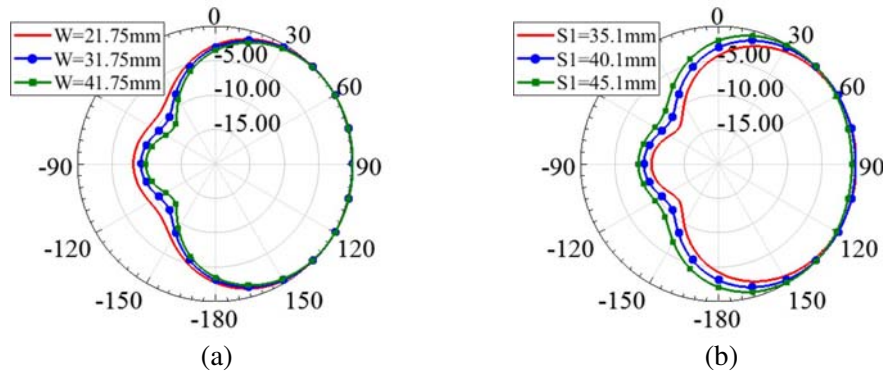
Figure 6. Effects of reflector width, W, (a) and separation, $S1$, (b) on co-pol azimuth patterns at 2.2 GHz.

(a)   (b)
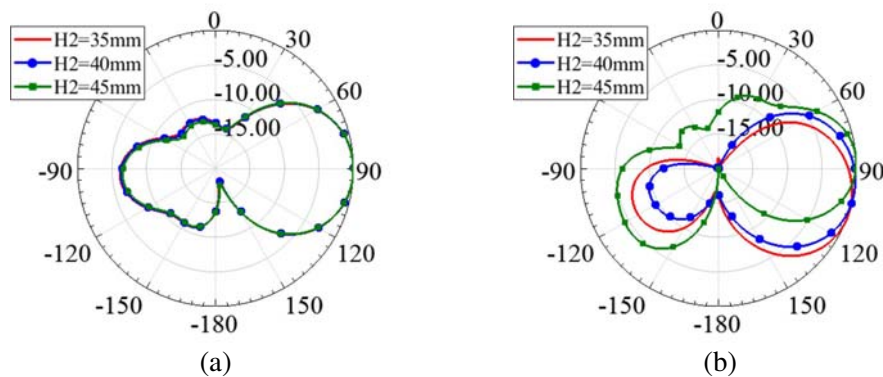
Figure 7. Effects of director length, $H2$, on co-pol elevation patterns ($\phi = 90°$) at 1.7 GHz (a) and 2.7 GHz (b).
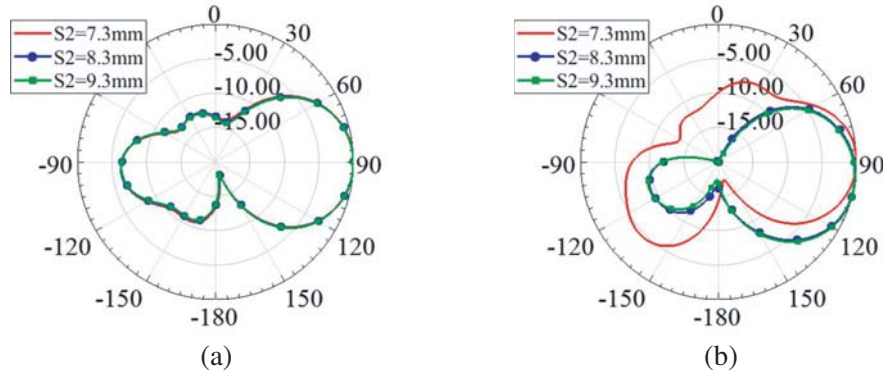
Figure 8. Effects of director separation, $S2$, on co-pol elevation patterns ($\phi = 90°$) at 1.7 GHz (a) and 2.7 GHz (b).
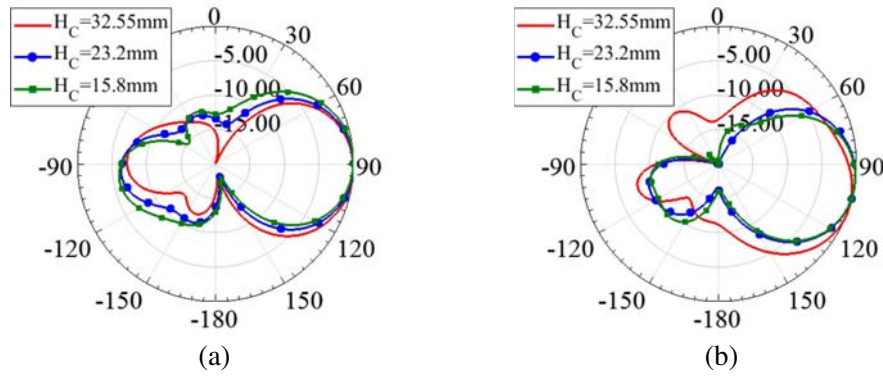
Figure 9. Effects of cable angle, H_C, on co-pol elevation patterns ($\phi = 90°$) at 1.7 GHz (a) and 2.7 GHz (b). Note that $\theta_C = 45°$ for $H_C = 32.55$ mm, $\theta_C = 55°$ for $H_C = 23.2$ mm, and $\theta_C = 65°$ for $H_C = 15.8$ mm.

impact on the elevation patterns. The biggest issue here is that the director loses its benefit as it is moved further and further from the sleeve.

The impacts of the cable angle, θ_C, and height, H_C, are shown in Fig. 9 where it is demonstrated that these parameters impact the elevation pattern performance over the entire operating band. This is due to currents that flow along the outer jacket of the feed cable. Notice that a cable angle and height of 45° and 32.55 mm provides a very deep null in the elevation pattern at 1.7 GHz but gives significant pattern distortion at 2.7 GHz. A cable angle and height of 65° and 15.8 mm has less impact on the overall patterns, but it increases the variation between the −10-dB crossover points which is not desirable. Note that the variations investigated for the pattern parametric study also have impacts on the peak gain and impedance match to the antenna. These impacts are not shown as part of this parametric study, but they should be considered in the antenna design. It is important to note that H_C is more critical than θ_C and has a much larger impact on the overall pattern performance.

4. RESULTS AND DISCUSSION

4.1. Simulated and Measured Results — Configuration A

A prototype configuration A antenna is fabricated and pictured in Fig. 10. Simulated and measured return losses for the wide-beam antenna are pictured in Fig. 10(e) where good agreement is shown between simulation and measurement. Measurements are taken with an Agilent E5071B network
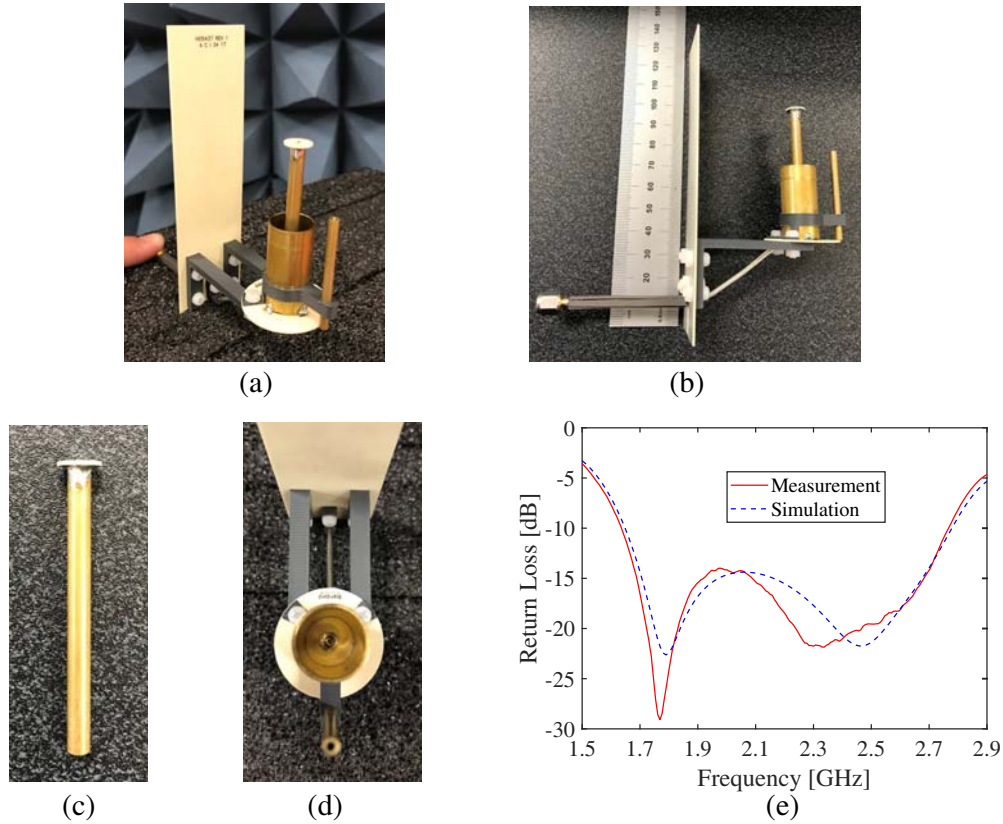
Figure 10. Fabricated antenna configuration A isometric view (a), side view (b), main radiator (c), threaded rod (d), and simulated and measured return losses (e).
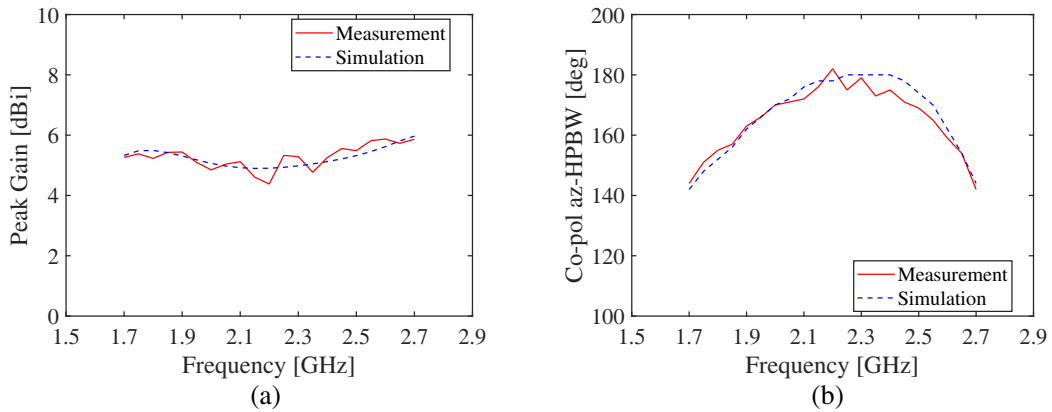
Figure 11. Configuration A simulated and measured gains (a) along with co-pol az-HPBW (b) vs. frequency.

analyzer. Measurements indicate a 10-dB return loss from roughly 1.64–2.76 GHz, and the return loss is better than 13 dB over the 1.7–2.7 GHz operating band. The simulated and measured gains and azimuth beamwidths are pictured in Fig. 11 where good agreement is observed between measured and simulated data. The radiation patterns are measured in an MVG SG 64 near-field range. The antenna exhibits measured peak gain between ~ 4.38–5.87 dBi, and the measured co-pol az-HPBW is between $\sim 142°$–182°. Note that the az-HPBW is measured at θ corresponding to the peak of the co-pol main beam. The measured front-to-back ratio ranges from roughly 6.7–10.3 dB [25]. The front-to-back ratio could
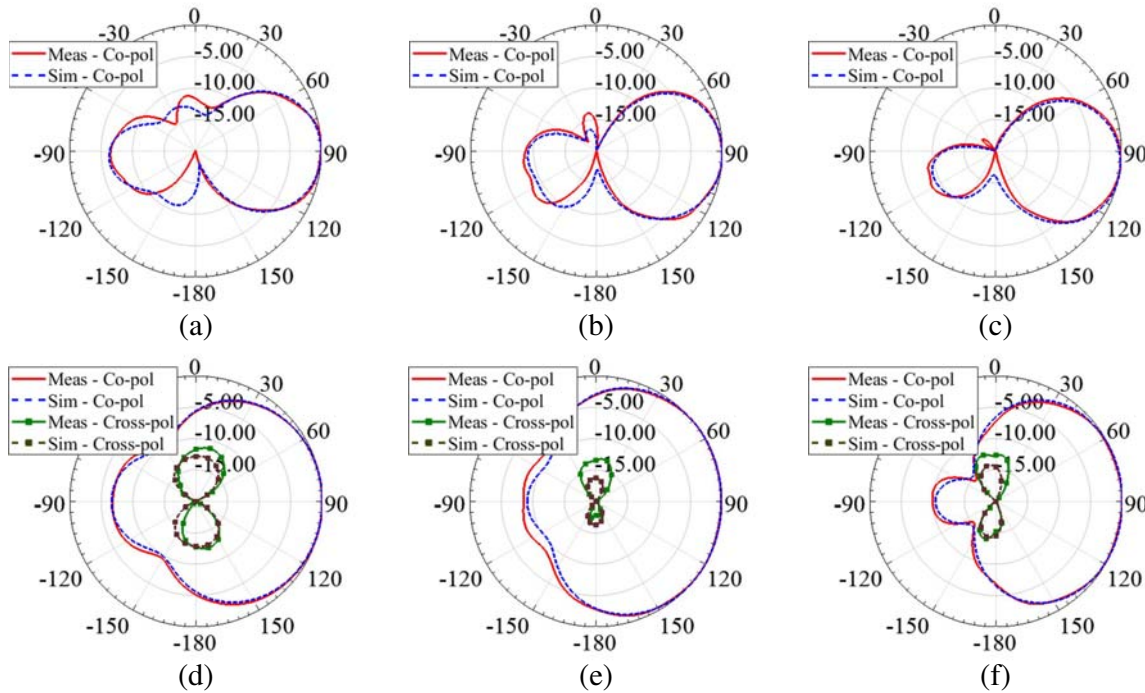
Figure 12. Simulated and measured radiation patterns for antenna configuration A. Elevation patterns are shown at 1.7 GHz (a), 2.2 GHz (b), and 2.7 GHz (c), and azimuth patterns are shown at 1.7 GHz (d), 2.2 GHz (e), and 2.7 GHz (f).

be improved by adding absorber material or an additional reflector behind the antenna. The antenna could also be arrayed in elevation to increase gain and improve front-to-back ratio. Unfortunately, all these methods would increase the overall size of the antenna.

The simulated and measured normalized radiation patterns are pictured in Fig. 12. Very good agreement is obtained between simulated and measured patterns where wide azimuth beamwidth is demonstrated. Also note that the antenna provides very good cross-polarization. The variations between simulation and measurement are likely due to manufacturing and assembly tolerances as well as range setup for the pattern measurements. The range cable is wrapped with absorber to minimize the impact to the radiation patterns, but it can still have a small impact. Some of the asymmetry observed in the cross-pol is likely due to the range cable. In all cases studied, the elevation patterns are plotted at $\phi = 90°$, and the azimuth patterns are plotted at θ corresponding to the measured peak of the co-pol main beam. For measured patterns, the co-pol main beam peak occurs at elevation angles of $\theta \simeq 85°$ (1.7 GHz), $\theta \simeq 97°$ (2.2 GHz), and $\theta \simeq 97°$ (2.7 GHz). For simulated patterns, the co-pol main beam peak occurs at elevation angles of $\theta \simeq 91°$ (1.7 GHz), $\theta \simeq 93°$ (2.2 GHz), and $\theta \simeq 101°$ (2.7 GHz).

4.2. Simulated and Measured Results — Configuration B

A fabricated configuration B antenna is pictured in Fig. 13, and the simulated and measured return losses are shown in Fig. 13(d). Note that aside from the main radiator, this is the same antenna as pictured in Fig. 10. Good agreement is obtained between simulation and measurement where the measured return loss is better than 19 dB from 1.9–2.4 GHz. The variations in return loss are likely due to fabrication and assembly tolerances primarily associated with the capacitive disk near the bottom of the main radiator.

The measured gain and azimuth beamwidth for antenna B are shown in Fig. 14 where the peak gain measures from $\sim$ 4.38–5.5 dBi, and the co-pol az-HPBW measures between $\sim$ 161° and 179°. The maximum beamwidth for antenna B is a bit more narrow than that for antenna A. This is due to the fact that there is slightly less squint for antenna B compared to antenna A due to the shorter main
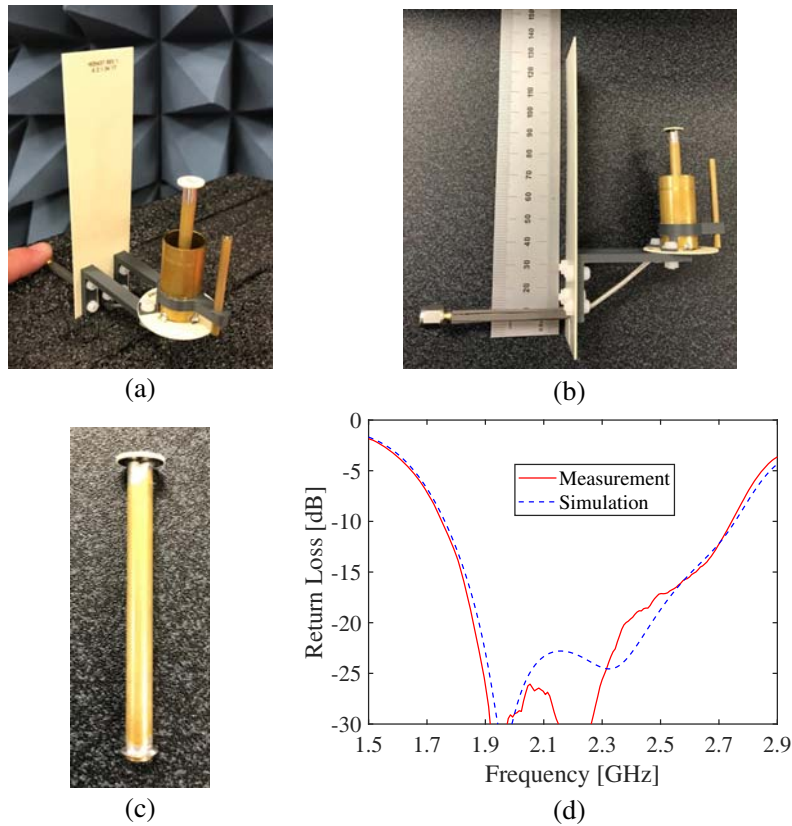
Figure 13. Fabricated antenna configuration B isometric view (a), side view (b), main radiator (c), and simulated and measured return losses (d).
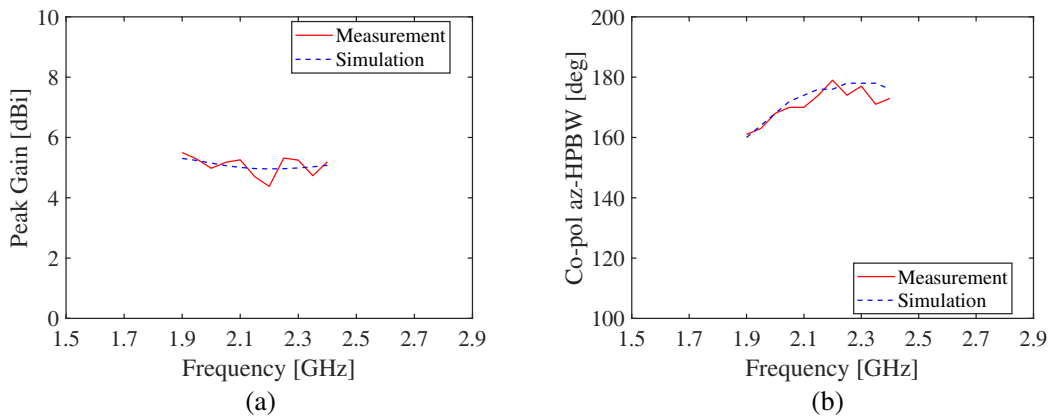
Figure 14. Configuration B simulated and measured gains (a) along with co-pol az-HPBW (b) vs. frequency.

radiator. As a result, more of the azimuth pattern is squeezed by the reflector creating a slightly more narrow azimuth pattern. The measured front-to-back ratio for antenna B ranges from roughly 8.1–9.5 dB [25] over the operating band. The normalized simulated and measured radiation patterns are shown in Fig. 15 where very good agreement is obtained between measurement and simulation. There are some small variations similar to those measured for antenna A. For measured patterns, the co-pol main beam peak occurs at $\theta \simeq 90°$ (1.9 GHz) and $\theta \simeq 96°$ (2.4 GHz). For simulated patterns, the co-pol main beam peak occurs at elevation angles of $\theta \simeq 92°$ (1.9 GHz) and $\theta \simeq 94°$ (2.4 GHz).
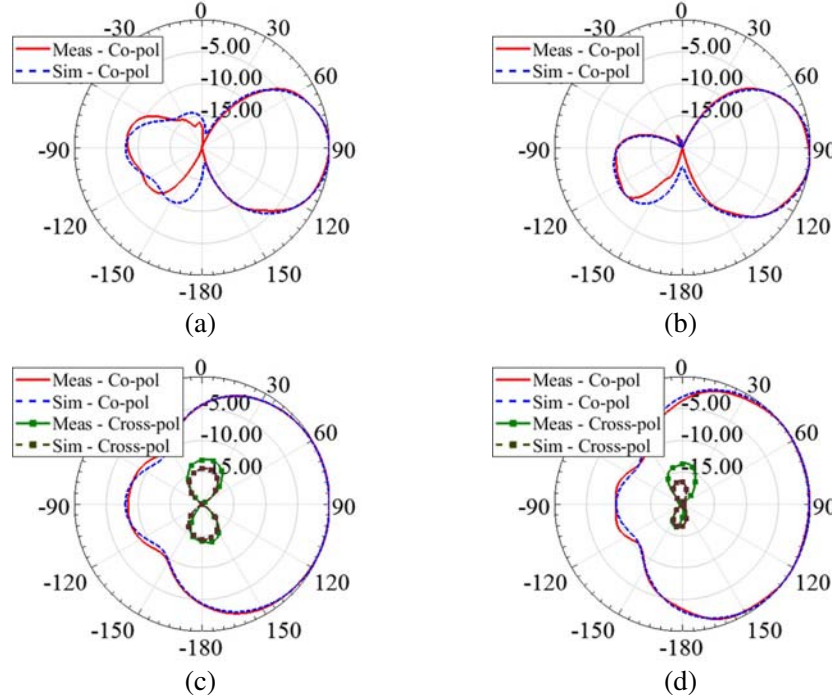
Figure 15. Simulated and measured radiation patterns for antenna configuration B. Elevation patterns are shown at 1.9 GHz (a) and 2.4 GHz (b), and azimuth patterns are shown at 1.9 GHz (c) and 2.4 GHz (d).

4.3. Comparison with Other Wide-Beam Antennas

Table 3 compares the wide-beam antenna in this paper to other linearly polarized wide-beam antennas presented in the literature. Compared to other approaches, the antenna in this paper provides broadband performance with respectable gain and relatively low spread in the azimuth beamwidth. Furthermore, this paper presents an antenna that is easily reconfigured for optimized return loss in different operating bands. Other wide-beam antennas presented in the literature do not provide the capability to easily tune the match for different bands while maintaining consistent wide-beam performance.

Table 3. Linearly polarized wide-beam antenna comparison.

	BW [%]	HPBW [deg]	Peak Gain [dBi]	Electrical Size [$\lambda_{mid\text{-}band}$]	Easily Reconfigured
This paper (A)	45	142–182	5.87	$0.94 \times 0.24 \times 0.54$	Yes (frequency)
This paper (B)	23	161–179	5.5	$0.94 \times 0.24 \times 0.54$	Yes (frequency)
[8]	15	221	2.23	$0.41 \times 0.43 \times 0.24$	No
[9]	18	130–148	8	$2.96 \times 1.58 \times 0.08$	No
[10]	3	188	2.86	$0.52 \times 0.52 \times 0.18$	No
[13]	85	60–150	7.1	Not provided	No
[14]	97	≤ 140	5.5	$0.39 \times 1 \times 0.74$	No
[15]	35	140–214	5.1	$0.51 \times 0.15 \times 0.16$	No
[16]	5	148	Not provided	$2 \times 2 \times 0.03$	No
[18]	86	> 150	9.2	$4.88 \times 4.88 \times 0.36$	No
[19]	7	196	4.52	$0.51 \times 0.51 \times 0.01$	Yes (pattern)

5. CONCLUSION

This paper presents a wide-beam antenna with a modular main radiator for base station applications. Two antenna variations are shown which are made possible with the modular main radiator. Antenna configuration A is considered the baseline antenna where the measured return loss is better than 13 dB and the azimuth beamwidth is between $\sim 142°$–$182°$ over the 1.7–2.7 GHz operating band. The benefit of a parasitic director coupled to the antenna is presented where the director improves the -10-dB crossover point compared to the antenna without a director. A second antenna, antenna configuration B, is presented for wide-beam performance from 1.9–2.4 GHz where the measured return loss is better than 19 dB. This versatile antenna is ideal for small cell base station and DAS applications requiring wide azimuth beamwidth, but the antenna could be useful in any application where in-situ antenna adjustment may be desirable.

REFERENCES

1. Nakamura, T., S. Nagata, A. Benjebbour, Y. Kishiyama, T. Hai, S. Xiaodong, Y. Ning, and L. Nan, "Trends in small cell enhancements in lte advanced," *IEEE Communications Magazine*, Vol. 51, 98–105, Feb. 2013.

2. Nasimuddin, Y. S. Anjani, and A. Alphones, "A wide-beam circularly polarized asymmetric-microstrip antenna," *IEEE Transactions on Antennas and Propagation*, Vol. 63, 3764–3768, Aug. 2015.

3. Ding, K., Y. Wang, and X. Xiong, "A novel wide-beam circularly polarized antenna for sdars applications," *IEEE Antennas and Wireless Propagation Letters*, Vol. 11, 811–813, 2012.

4. Wen, Y., B. Wang, and X. Ding, "Wide-beam circularly polarized microstrip magnetic-electric dipole antenna for wide-angle scanning phased array," *IEEE Antennas and Wireless Propagation Letters*, Vol. 16, 428–431, 2017.

5. Pan, Z., W. Lin, and Q. Chu, "Compact wide-beam circularly-polarized microstrip antenna with a parasitic ring for cnss application," *IEEE Transactions on Antennas and Propagation*, Vol. 62, 2847–2850, May 2014.

6. Ta, S. X. and I. Park, "Crossed dipole loaded with magneto-electric dipole for wideband and wide-beam circularly polarized radiation," *IEEE Antennas and Wireless Propagation Letters*, Vol. 14, 358–361, 2015.

7. Sun, L., B.-H. Sun, H. Wu, J. Yuan, and W. Tang, "Broadband, wide beam circularly polarized antenna with a novel matching structure for satellite communications," *Progress In Electromagnetics Research C*, Vol. 59, 159–166, 2015.

8. Yang, G., J. Li, S. G. Zhou, and Y. Qi, "A wide-angle e-plane scanning linear array antenna with wide beam elements," *IEEE Antennas and Wireless Propagation Letters*, Vol. 16, 2923–2926, 2017.

9. Wen, Y., B. Wang, and X. Ding, "Wide-beam siw-slot antenna for wide-angle scanning phased array," *IEEE Antennas and Wireless Propagation Letters*, Vol. 15, 1638–1641, 2016.

10. Cheng, Y., X. Ding, W. Shao, M. Yu, and B. Wang, "2-d planar wide-angle scanning-phased array based on wide-beam elements," *IEEE Antennas and Wireless Propagation Letters*, Vol. 16, 876–879, 2017.

11. Kedar, A. and K. Beenamole, "Wide beam tapered slot antenna for wide angle scanning phased array antenna," *Progress In Electromagnetics Research B*, Vol. 27, 235–251, 2011.

12. Bai, Y.-Y., S. Xiao, M.-C. Tang, Z.-F. Ding, and B.-Z. Wang, "Wide-angle scanning phased array with pattern reconfigurable elements," *IEEE Transactions on Antennas and Propagation*, Vol. 59, no. 11, 4071–4076, 2011.

13. Eldek, A. A., "Design of double dipole antenna with enhanced usable bandwidth for wideband phased array applications," *Progress In Electromagnetics Research*, Vol. 59, 1–15, 2006.

14. Wang, J., L. Zhou, and W. Chen, "A novel wide beam UWB antenna," *2010 International Conference on Microwave and Millimeter Wave Technology*, 961–964, May 2010.

15. He, Y., W. Wang, H. Yang, and X. Du, "Improved design of a broadband dielectric resonator antenna with wide beam," *International Journal of Antennas and Propagation*, Vol. 2018, 7, 2018.

16. Wang, R., B.-Z. Wang, C. Hu, C. Gong, and X. Ding, "Low-profile on-board antenna with a broad beam based on three-current model," *Progress In Electromagnetics Research*, Vol. 156, 13–24, 2016.

17. Qi, Z., J. Kuai, Y. Zhou, and W. Hong, "A wide beam, dual polarization and high gain antenna for WCDMA base station application," *Microwave Conference Proceedings, 2005. APMC 2005. Asia-Pacific Conference Proceedings*, Vol. 4, 3, IEEE, 2005.

18. Nakano, H., Y. Ogino, and J. Yamauchi, "Bent two-leaf antenna radiating a tilted, linearly polarized, wide beam," *IEEE Transactions on Antennas and Propagation*, Vol. 58, No. 11, 3721–3725, 2010.

19. Gao, M., B. Wang, Y. Li, and B. Tian, "A new pattern reconfigurable loop antenna with wide beam width," *2018 Cross Strait Quad-Regional Radio Science and Wireless Technology Conference (CSQRWC)*, 1–3, Jul. 2018.

20. Gong, L., K. Y. Chan, and R. Ramer, "A reconfigurable spiral antenna with wide beam coverage," *2013 IEEE Antennas and Propagation Society International Symposium (APSURSI)*, 206–207, Jul. 2013.

21. Huang, P., Q. Guo, Z.-Y. Zhang, Y. Li, and G. Fu, "Design of a wideband sleeve antenna with symmetrical ridges," *Progress In Electromagnetics Research Letters*, Vol. 55, 137–143, 2015.

22. Li, Y., Z.-Y. Zhang, Q.-Q. Liu, Y.-X. Zhang, and G. Fu, "A novel wideband sleeve antenna with capacitive annulus for wireless communication," *Progress In Electromagnetics Research C*, Vol. 52, 1–6, 2014.

23. Shehan, J. W. and R. S. Adams, "Sleeve monopole antenna with integrated filter for base station applications," *2017 USNC-URSI Radio Science Meeting (Joint with AP-S Symposium)*, 11–12, Jul. 2017.

24. Dixon, P., "Cavity-resonance dampening," *IEEE Microwave Magazine*, Vol. 6, 74–84, Jun. 2005.

25. BASTA, "Recommendation on base station antenna standards," White Paper — BASTA, Feb. 2017.